Modelling and simulation of radiative heat transfer in non-grey absorbing and emitting media under phase change

Fatima-Ezzahrae Moutahir[a], Youssef Belhamadia[b,*], Mohammed Seaid[c], Mofdi El-Amrani[a]

[a] *Mathematics and Applications Laboratory, FST, Abdelmalek Essaadi University, Tangier, Morocco*
[b] *American University of Sharjah, Department of Mathematics and Statistics, Sharjah, United Arab Emirates*
[c] *Department of Engineering, University of Durham, South Road, DH1 3LE, United Kingdom*

Abstract

A class of mathematical models are proposed for modelling and numerical simulation of coupled radiative and conductive heat transfer in non-grey absorbing and emitting media under phase change. Progress in this area of mathematical modelling would contribute to a sustainable future manufacturing involving high temperature and phase change. Accurately predicting phase-change interface is the crucial step for these applications in non-grey semi-transparent media. In the present study, the conduction and radiation effects are analyzed by a set of nonlinear partial differential equations and a linear integral equation, respectively. The proposed model forms a system of nonlinear integro-differential equations and it accounts for both thermal radiation and phase change in the design. For non-grey media, the spectrum is divided into a sequence of finite intervals of frequency bands with averaged absorption coefficients resulting in coupled systems to be solved for each frequency band. The coupled equations are approximated using a second-order method in both time and space. Using discrete ordinates for the angular discretization of the integral equation for the radiation effects, a Newton-type algorithm is used to deal with the nonlinear systems. Numerical results are presented for several test problems in both grey and non-grey media, and comparisons to simulations without radiation are also shown in this study. The findings here could be used to understand effects of thermal radiation in non-grey absorbing and emitting media under phase change.

Keywords: Radiative heat transfer; Phase change; Discrete ordinates; Source iteration; Newton method; Non-grey media.

Nomenclature

ρ_s	solid density, $(kg \cdot m^{-3})$	L	latent heat of fusion, $(J \cdot kg^{-1})$
ρ_l	liquid density, $(kg \cdot m^{-3})$	c_s	solid specific heat, $(J \cdot kg^{-1} \cdot K)$

*Corresponding author
Email addresses: fatimaezzahrae.moutahir@etu.uae.ac.ma (Fatima-Ezzahrae Moutahir), ybelhamadia@aus.edu (Youssef Belhamadia), m.seaid@durham.ac.uk (Mohammed Seaid), mofdi.elamrani@urjc.es (Mofdi El-Amrani)

c_l	liquid specific heat, $(J \cdot kg^{-1} \cdot K)$
K_s	solid thermal conductivity, $(W \cdot m^{-1} \cdot K^{-1})$
K_l	liquid thermal conductivity, $(W \cdot m^{-1} \cdot K^{-1})$
h_c	convective heat coefficient, $(J \cdot kg^{-1} \cdot K^{-1})$
V_Γ	interface normal velocity, $(m \cdot s^{-1})$
α	emissivity
κ	absorption coefficient, (m^{-1})
σ	scattering coefficient, (m^{-1})
ν	frequency variable, (μm^{-1})
$\boldsymbol{s}$	angular direction
ψ	intensity, $(J \cdot m^{-2} \cdot \mu m)$
φ	mean intensity, $(J \cdot m^{-2})$
T	temperature, (K)
T_f	fusion temperature, (K)
B	Planck function, $(W \cdot m^{-2} \cdot \mu m^{-1})$
h_p	Planck constant, $(J \cdot s)$
k_B	Boltzmann constant, $(J \cdot K^{-1})$
a_R	Stefan–Boltzmann constant, $(W \cdot m^{-2} \cdot K^4)$
T_b	surround medium temperature, (K)
T_0	initial temperature, (K)
t	time, (s)
$\mathbf{x}$	spatial coordinate, (m)
Ω	spatial domain
$\partial\Omega$	domain boundary
$\mathbb{S}^2$	unit sphere
$\mathbf{n}$	surface normal
c_0	speed of light in vacuum, $(m \cdot s^{-1})$

1. Introduction

In many industrial and engineering thermal applications, radiative heat transfer is present and strongly influences the thermal features of the final product. This is especially the case in all industrial applications that involve high temperatures, such as iron and steel manufacturing [1, 2], glass manufacturing [3], gas turbine combustion chambers [4], among others. Particular attention is paid to applications that involve phase change in materials as in crystal growth [5] and continuous casting [6, 7]. In this type of applications, in addition to radiation, the heat exchange at the liquid-solid interface often plays a crucial role and affects the shape and structure of the desired material. These problems are complex and their experimental investigations can be extremely difficult to carry out and very demanding to achieve. Therefore, it is of great interest to develop mathematical models and accurate numerical methods for studying and simulating such coupled radiative phase-change problems in participating media. Mathematical modelling of effects of the radiation in phase change problems presents big challenges due to the complex interactions of radiation, heat transfer, fluid flow, and heat exchange between liquid and solid. The first mathematical model for liquid-solid phase change phenomena was proposed by Josef Stefan in 1891 [8]. However, we had to wait till 1970s when effects of internal radiation upon phase change of semi-transparent materials began to be studied, where the

classical Stefan problem has been reformulated to include radiative transfer, see for instance [9, 10]. In 1983, the classical Stefan problem was reformulated by authors in [11] to include radiative transfer not only in the solid and liquid zones but in the mushy region between them as well. It should be pointed out that in these contributions, only one-dimensional geometry was performed. In 1988, authors in [12] employed the enthalpy formulation for the heat in order to obtain a more general solution of the multidimensional Stefan problem, when including internal radiation of semi-transparent materials. In this approach, the interface liquid-solid condition, well known by the Stefan condition, is implicitly satisfied and the energy equation is applied over the entire computational domain covering both liquid and solid phases.

Since 1990, applied numerical modeling of coupling phase-change heat transfer and radiation in semi-transparent media is ascending. Both, Stefan problem and enthalpy formulation, have been used to study effects of the internal radiative heat transfer in phase change materials. However, to our knowledge the existing contributions consider only semi-transparent grey media. For instance, in [13] modelling of a two-dimensional transient solidification process of semi-transparent materials was undertaken. The enthalpy formulation was used for the energy equation and the finite volume method was used to solve the radiative heat transfer. In [14], the conduction-radiation controlled solidification process of semi-transparent materials was numerically analyzed based on the fixed grid front-tracking method, where the governing energy and the radiative equations were solved implicitly on a fixed mesh and the interface was tracked explicitly. In [15] a coupled heat transfer of solidification and radiation within a two-dimensional rectangular semi-transparent medium having gradient index was investigated. The three phase-change zones namely, liquid, solid, and mushy-zones, were included. A Galerkin finite element method was used to solve the energy equation of the coupled radiation and phase-change heat transfer. Authors in [16] were first to model both convection and radiation in phase change materials by reformulating the enthalpy formulation. In addition, recently inverse problems of radiative heat transfer and phase change in semi-transparent media without convection have been introduced in the literature using an improved stochastic particle swarm optimization algorithm, see [17, 18] among others.

There is a general agreement in the literature that coupling radiative heat transfer and phase change is numerically very complicated and highly demanding. Many numerical methods have been used in the literature including different standard methods such as lattice Boltzmann methods [**?** **?**], finite volume methods [14**?**], finite element methods [15], and finite difference methods [**?**] for phase-change applications in semi-transparent materials. While using these methods to solve the energy formulation, the radiative transfer equation has been solved by using the well-established discrete transfer method [**?**], the discrete-ordinates method [**?**], the spherical harmonics method [**?**], and the simplified spherical harmonics method [19]. This literature review is not exhaustive but, to our knowledge the divergence of radiative heat flux vector is calculated only for a grey medium for these references. The main objective of the current study is to present robust techniques for mathematical modelling and numerical simulation of the coupling phase-change heat transfer and radiation in a non-grey absorbing and emitting media. The proposed novel formulation couples the enthalpy technique for phase change [20, 21] with a set of nonlinear integro-differential equations accounting for thermal radiation [22]. Given the optical spectrum of the participating non-grey media,

a frequency-averaged approach is adopted in this study to divide the spectrum interval into a finite set of bands with piecewise constant absorption and scattering coefficients. Hence, the full radiative heat transfer equation is transformed into a series of coupled nonlinear equations to be solved for the averaged spectral intensity according to an averaged Planck function. Using the discrete-ordinates method for the angle discretization, an upwind method for the space discretization. The discrete-ordinates method is a well established method for solving the radiative model. For instance, it has been recently used for solving the coupled radiation and conduction heat transfer equations in [**?** **?**] and to solve the time-domain radiative transfer equation in [**?** **?**]. The fully coupled model is discretized using second-order methods in both time and space. The discretized problem yields a nonlinear system to be solved for the mean spectral intensity and temperature distribution. The obtained system is solved using a Newton-type algorithm at each time step. The proposed numerical solver is expected to be unconditionally stable and consistently accurate for a wide range of applications for heat transfer process in non-grey absorbing and emitting media under phase change. Numerical results are presented for two test problems in both grey and non-grey media, and comparisons to simulations without radiation are also performed. Combining the present approach with physics-based computer modeling can provide a potential tool for design of coupled radiative and conductive heat transfer in a non-grey absorbing and emitting medium under phase change.

The present paper is organized as follows. The equations employed for modelling conductive heat transfer in non-grey absorbing and emitting media under phase change are discussed in section 2. In section 3 we present the formulation of the fully implicit method on staggered grids for the solution procedure. This section includes the formulation of discrete ordinates, discretization of the radiative transfer equation, the space and time discretizations of the nonlinear heat equation, and the solver implementation for the fully coupled problem. Section 4 is devoted to the numerical performance of the proposed method using two examples of coupled radiative and conductive heat transfer in a non-grey absorbing and emitting media under phase change. Our approach is demonstrated to enjoy the expected efficiency as well as accuracy and stability. Concluding remarks are summarized in section 5.

2. Mathematical models for radiative heat transfer under phase change

In a general framework, modelling thermal radiation in non-grey media requires integro-differential equations involving the space, direction and frequency variables due to the energy transport by photons, see for example [23, 24, 25] among others. In the presence of phase change, the radiation model should be combined with the classical Stefan problem that describes the evolution of the liquid-solid interface of a material undergoing a phase change, see for example [9, 11]. The model consists of a heat equation for the temperature $T(\boldsymbol{x}, t)$ and a transport equation for the radiative intensity $\psi(\boldsymbol{x}, \boldsymbol{s}, \nu)$. Given a spatial solid domain Ω_s, liquid domain Ω_l, liquid-solid interface $\Gamma(t)$, and a time

interval $[0, t_f]$, the governing equations read

$$\begin{cases} \rho_s c_s \dfrac{\partial T}{\partial t} - \nabla \cdot (\boldsymbol{K}_s \nabla T) &= -\displaystyle\int_{\nu_0}^{\infty} \kappa_s(\nu) \left(4\pi B(T,\nu) - \int_{\mathbb{S}^2} \psi(\boldsymbol{x}, \boldsymbol{s}, \nu) d\boldsymbol{s} \right) d\nu, & (\boldsymbol{x}, t) \in \Omega_s \times [0, t_f], \\ \rho_l c_l \dfrac{\partial T}{\partial t} - \nabla \cdot (\boldsymbol{K}_l \nabla T) &= -\displaystyle\int_{\nu_0}^{\infty} \kappa_l(\nu) \left(4\pi B(T,\nu) - \int_{\mathbb{S}^2} \psi(\boldsymbol{x}, \boldsymbol{s}, \nu) d\boldsymbol{s} \right) d\nu, & (\boldsymbol{x}, t) \in \Omega_l \times [0, t_f], \\ \boldsymbol{s} \cdot \nabla \psi + \Big(\kappa_s(\nu) + \sigma_s(\nu) \Big) \psi &= \dfrac{\sigma_s(\nu)}{4\pi} \displaystyle\int_{\mathbb{S}^2} \psi(\boldsymbol{x}, \boldsymbol{s}, \nu) d\boldsymbol{s} + \kappa_s(\nu) B(T, \nu), & (\boldsymbol{x}, \nu, \boldsymbol{s}) \in \Omega_s \times [\nu_0, \infty[\times \mathbb{S}^2, \\ \boldsymbol{s} \cdot \nabla \psi + \Big(\kappa_l(\nu) + \sigma_l(\nu) \Big) \psi &= \dfrac{\sigma_l(\nu)}{4\pi} \displaystyle\int_{\mathbb{S}^2} \psi(\boldsymbol{x}, \boldsymbol{s}, \nu) d\boldsymbol{s} + \kappa_l(\nu) B(T, \nu), & (\boldsymbol{x}, \nu, \boldsymbol{s}) \in \Omega_l \times [\nu_0, \infty[\times \mathbb{S}^2, \\ T(\boldsymbol{x}, t) &= T_f(\boldsymbol{x}, t), & (\boldsymbol{x}, t) \in \Gamma(t) \times [0, t_f], \\ \psi(\boldsymbol{x}, \boldsymbol{s}, \nu) &= B(T_f, \nu), & (\boldsymbol{x}, \boldsymbol{s}, \nu) \in \Gamma(t) \times \Omega_s \times [\nu_0, \infty[, \\ \Big(\boldsymbol{K}_s \boldsymbol{\nabla} T \Big) \cdot \boldsymbol{n}_s - (\boldsymbol{K}_l \boldsymbol{\nabla} T) \cdot \boldsymbol{n}_l &= \rho_l L V_\Gamma, & (\boldsymbol{x}, t) \in \Gamma(t) \times [0, t_f]. \end{cases} \tag{1}$$

The boundary and initial conditions are given by

$$\begin{cases} \boldsymbol{K}_s \boldsymbol{n}(\hat{\boldsymbol{x}}) \cdot \nabla T + h_c (T - T_b) &= \alpha\pi \displaystyle\int_0^{\nu_0} \Big(B(T_b, \nu) - B(T, \nu) \Big) d\nu, & (\hat{\boldsymbol{x}}, t) \in \partial\Omega_s \times [0, t_f], \\ \boldsymbol{K}_l \boldsymbol{n}(\hat{\boldsymbol{x}}) \cdot \nabla T + h_c (T - T_b) &= \alpha\pi \displaystyle\int_0^{\nu_0} \Big(B(T_b, \nu) - B(T, \nu) \Big) d\nu, & (\hat{\boldsymbol{x}}, t) \in \partial\Omega_l \times [0, t_f], \\ \psi(\hat{\boldsymbol{x}}, \boldsymbol{s}, \nu) &= B(T_b, \nu), & (\hat{\boldsymbol{x}}, \nu, \boldsymbol{s}) \in \partial\Omega^- \times [0, \nu_0[\times \mathbb{S}^2, \\ T(\boldsymbol{x}, 0) &= T_0(\boldsymbol{x}), & \boldsymbol{x} \in \Omega. \end{cases} \tag{2}$$

Here, $B(T, \nu, n)$ is the spectral intensity of the black-body radiation defined by the Planck function as [22]

$$B(T, \nu) = \frac{2 h_P \nu^3}{c_0^2} \frac{1}{\exp\left(\dfrac{h_P \nu}{\kappa_B T} \right) - 1}. \tag{3}$$

Note that on the boundary, we consider the transmitting conditions where the boundary region $\partial\Omega^-$ is defined as

$$\partial\Omega^- = \Big\{ \hat{\boldsymbol{x}} \in \partial\Omega : \quad \mathbf{n}(\hat{\boldsymbol{x}}) \cdot \boldsymbol{s} < 0 \Big\}.$$

The major difficulty in the system (1) lies on the fact that the interface $\Gamma(t)$ and its velocity V_Γ are not known a priori and they also evolve with time. To overcome this challenge, a new formation over the whole computational domain $\Omega = \Omega_s \cup \Omega_l \cup \Gamma(t)$ is introduced. One way to do so is to start with the enthalpy formulation as follows

$$\begin{cases} \dfrac{\partial H}{\partial t} - \nabla \cdot \Big(\mathcal{K}(T) \nabla T \Big) &= -\displaystyle\int_{\nu_0}^{\infty} \kappa(\nu) \left(4\pi B(T,\nu) - \int_{\mathbb{S}^2} \psi(\boldsymbol{x}, \boldsymbol{s}, \nu) d\boldsymbol{s} \right) d\nu, & (\boldsymbol{x}, t) \in \Omega \times [0, t_f], \\ \boldsymbol{s} \cdot \nabla \psi + \Big(\kappa(\nu) + \sigma(\nu) \Big) \psi &= \dfrac{\sigma(\nu)}{4\pi} \displaystyle\int_{\mathbb{S}^2} \psi(\boldsymbol{x}, \boldsymbol{s}, \nu) d\boldsymbol{s} + \kappa(\nu) B(T, \nu), & (\boldsymbol{x}, \boldsymbol{s}, \nu) \in \Omega \times \mathbb{S}^2 \times [\nu_0, \infty[, \end{cases} \tag{4}$$

where H is the enthalpy defined by

$$H = \begin{cases} \rho_s c_s T, & \text{if} \quad T < T_f, \\ \rho_l L + \rho_s c_s T_f + \rho_l c_l (T - T_f), & \text{if} \quad T > T_f, \end{cases} \qquad \kappa(\nu) = \begin{cases} \kappa_s(\nu), & \text{if} \quad T < T_f, \\ \kappa_l(\nu), & \text{if} \quad T > T_f, \end{cases}$$

and

$$\sigma(\nu) = \begin{cases} \sigma_s(\nu), & \text{if} \quad T < T_f, \\ \\ \sigma_l(\nu), & \text{if} \quad T > T_f. \end{cases}$$

It should be noted that the problem (4) is equivalent to (1) and it preserves the main advantage that the interface conditions are automatically satisfied. In contrast to the approach used in [13, 15, 17], we employed a different method for our proposed full radiative-phase-change model. We introduced an interface function ϕ in a similar way to that presented in [20]. We then proceeded to use the following decomposition:

$$H = H_1 + \rho_l L\phi, \tag{5}$$

where H_1 is now a continuous function defined by

$$H_1 = \begin{cases} \rho_s c_s T, & \text{in } \Omega_s, \\ \\ \rho_s c_s T_f + \rho_l c_l (T - T_f), & \text{in } \Omega_l, \end{cases} \qquad \text{and} \qquad \phi = \begin{cases} 0, & \text{in } \Omega_s, \\ \\ 1, & \text{in } \Omega_l. \end{cases}$$

Replacing the equation (5) in the system (4), a new formulation is obtained which is also equivalent to the classical Stefan problem as

$$\begin{cases} \alpha(\phi)\dfrac{\partial T}{\partial t} + \rho L \dfrac{\partial \phi}{\partial t} - \nabla \cdot \Big(\mathcal{K}_c(\phi)\nabla T\Big) &= -\displaystyle\int_{\nu_0}^{\infty} \kappa_\phi(\nu)\left(4\pi B(T,\nu) - \int_{\mathbb{S}^2} \psi(\boldsymbol{x},\boldsymbol{s},\nu)d\boldsymbol{s}\right)d\nu, \quad (\boldsymbol{x},t) \in \Omega \times [0,t_f], \\ \\ \boldsymbol{s}\cdot\nabla\psi + \Big(\kappa_\phi(\nu) + \sigma_\phi(\nu)\Big)\psi &= \dfrac{\sigma_\phi(\nu)}{4\pi}\displaystyle\int_{\mathbb{S}^2} \psi(\boldsymbol{x},\boldsymbol{s},\nu)d\boldsymbol{s} + \kappa_\phi(\nu)B(T,\nu), \qquad (\boldsymbol{x},\boldsymbol{s},\nu) \in \Omega \times \mathbb{S}^2 \times [\nu_0,\infty[, \end{cases} \tag{6}$$

where

$$\alpha(\phi) = \rho_s c_s + \phi\Big(\rho_l c_l - \rho_s c_s\Big), \qquad \mathcal{K}_c(\phi) = \boldsymbol{K}_s + \phi\Big(\boldsymbol{K}_l - \boldsymbol{K}_s\Big), \qquad f(\phi) = f_s + \phi\Big(f_l - f_s\Big),$$

$$\kappa_\phi(\nu) = \kappa_s(\nu) + \phi\Big(\kappa_l(\nu) - \kappa_s(\nu)\Big), \qquad \sigma_\phi(\nu) = \sigma_s(\nu) + \phi\Big(\sigma_l(\nu) - \sigma_s(\nu)\Big).$$

In practical applications, phase change occurs in a small temperature range $[T_f - \epsilon, T_f + \epsilon]$, with ϵ is a given constant assumed to be small in our simulations. Thus, ϕ can be replaced by a regularised function $F_\epsilon(T)$ and in this study we consider

$$\phi = F_\epsilon(T) = \frac{1}{2} - \frac{1}{2}\tanh\left(\frac{T_f - T}{\epsilon}\right).$$

Therefore, the proposed full radiative-phase-change model is formulated as

$$\begin{cases} \alpha(T)\dfrac{\partial T}{\partial t} + \rho L \dfrac{\partial F_\epsilon(T)}{\partial t} - \nabla \cdot \Big(\mathcal{K}_c(T)\nabla T\Big) &= -\displaystyle\int_{\nu_0}^{\infty} \kappa_\phi(\nu)\left(4\pi B(T,\nu) - \int_{\mathbb{S}^2} \psi(\boldsymbol{x},\boldsymbol{s},\nu)d\boldsymbol{s}\right)d\nu, \quad (\boldsymbol{x},t) \in \Omega \times [0,t_f], \\ \\ \boldsymbol{s}\cdot\nabla\psi + \Big(\kappa_\phi(\nu) + \sigma_\phi(\nu)\Big)\psi &= \dfrac{\sigma_\phi(\nu)}{4\pi}\displaystyle\int_{\mathbb{S}^2} \psi(\boldsymbol{x},\boldsymbol{s},\nu)d\boldsymbol{s} + \kappa_\phi(\nu)B(T,\nu), \qquad (\boldsymbol{x},\boldsymbol{s},\nu) \in \Omega \times \mathbb{S}^2 \times [\nu_0,\infty[, \end{cases} \tag{7}$$

equipped with the following boundary and initial conditions

$$\begin{cases} \mathcal{K}_c(T)\boldsymbol{n}(\hat{\boldsymbol{x}})\cdot\nabla T + h_c(T-T_b) &= \alpha\pi\displaystyle\int_0^{\nu_0}\Big(B(T_b,\nu)-B(T,\nu)\Big)d\nu, & (\hat{\boldsymbol{x}},t)\in\partial\Omega\times[0,t_f],\\ \psi(\hat{\boldsymbol{x}},\boldsymbol{s},\nu) &= B(T_b,\nu), & (\hat{\boldsymbol{x}},\nu,\boldsymbol{s})\in\partial\Omega^-\times[0,\nu_0[\times\mathbb{S}^2,\\ T(\boldsymbol{x},0) &= T_0(\boldsymbol{x}), & \boldsymbol{x}\in\Omega. \end{cases} \tag{8}$$

To deal with the non-grey medium in the above radiative-phase-change equations, a numerical method is required for a discretization of the radiative spectrum $[\nu_0,\infty)$. There exists various techniques in the literature to perform this step including the line-by-line, narrow-band model, wide-band model and full spectrum methods, see [26, 27, 28, 29] among others. However, these methods have been widely used for reacting non-grey media which occur mainly in combustion and reactive flows with several non-grey chemical species. For a detailed discussion of the performance of these methods for resolving non-grey properties in radiative heat transfer, we refer to [30] and further references are therein. Since the media considered in the present study is non-reactive, we consider a simple frequency-averaged method to resolve the non-grey medium. Hence, Following ideas reported for instance in [31, 32], the radiative spectrum $[\nu_0,\infty)$ is divided into a finite set of small intervals $[\nu_{k-1},\nu_k)$ and we assume that the spectral absorption coefficients $\kappa(\nu)$ are piecewise constants with respect to the frequency ν *i.e.*,

$$\kappa_\phi(\nu)=\kappa_\phi^{(k)},\qquad \sigma_\phi(\nu)=\sigma_\phi^{(k)},\qquad \forall\ \nu\in[\nu_{k-1},\nu_k),\quad k=1,2,\ldots,N_f, \tag{9}$$

with κ_k and σ_k are constants, and N_f is the total number of spectral bands. We also define the frequency-averaged intensity in the band $[\nu_{k-1},\nu_k]$ by

$$\psi^{(k)}(\boldsymbol{x},\boldsymbol{s})=\int_{\nu_{k-1}}^{\nu_k}\psi(\boldsymbol{x},\boldsymbol{s},\nu)d\nu. \tag{10}$$

If we introduce the mean intensity $\varphi^{(k)}(\boldsymbol{x})$ and the averaged Planck function $B^{(k)}$ in the kth spectral band

$$\varphi^{(k)}(\boldsymbol{x})=\int_{\nu_{k-1}}^{\nu_k}\psi^{(k)}(\boldsymbol{x},\boldsymbol{s},\nu)d\boldsymbol{s},\qquad B^{(k)}(T)=\int_{\nu_{k-1}}^{\nu_k}B(T,\nu)d\nu,\qquad k=1,2,\ldots,N_f, \tag{11}$$

then, the full radiative-phase-change problem (7)-(8) transforms to

$$\begin{cases} \alpha(T)\dfrac{\partial T}{\partial t}+\rho L\dfrac{\partial F_\epsilon(T)}{\partial t}-\nabla\cdot(\mathcal{K}_c(T)\nabla T) &= -\displaystyle\sum_{k=1}^{N_f}\kappa_\phi^{(k)}\left(4\pi B^{(k)}(T)-\varphi^{(k)}\right), & (\boldsymbol{x},t)\in\Omega\times[0,t_f],\\ \boldsymbol{s}\cdot\nabla\psi^{(k)}+\left(\kappa_\phi^{(k)}+\sigma_\phi^{(k)}\right)\psi^{(k)} &= \dfrac{\sigma_\phi^{(k)}}{4\pi}\varphi^{(k)}+\kappa_\phi^{(k)}B^{(k)}(T), & (\boldsymbol{x},\boldsymbol{s})\in\Omega\times\mathbb{S}^2, k=1,\ldots,N_f,\\ \mathcal{K}_c\boldsymbol{n}(\hat{\boldsymbol{x}})\cdot\nabla T+h_c(T-T_b) &= \alpha\pi\Big(B^{(0)}(T_b)-B^{(0)}(T)\Big), & (\hat{\boldsymbol{x}},t)\in\partial\Omega\times[0,t_f],\\ \psi^{(k)}(\hat{\boldsymbol{x}},\boldsymbol{s}) &= B^{(k)}(T_b), & (\hat{\boldsymbol{x}},\boldsymbol{s})\in\partial\Omega^-\times\mathbb{S}^2, k=1,\ldots,N_f,\\ T(\boldsymbol{x},0) &= T_0(\boldsymbol{x}), & \boldsymbol{x}\in\Omega. \end{cases} \tag{12}$$

Note that since the medium is assumed to be formed with a single material with a given optical spectrum, using more advanced approximations such as line-by-line or wide-band models would not improve the overall accuracy of the considered approach. It should also be stressed that for a grey medium, the Planck function reduces to

$$B(T) = a_R T^4,$$

and the coupled radiative and conductive heat transfer under phase change becomes

$$\begin{cases} \alpha(T)\dfrac{\partial T}{\partial t} + \rho L \dfrac{\partial F_\epsilon(T)}{\partial t} - \nabla \cdot \Big(\mathcal{K}_c(T)\nabla T\Big) &= -\kappa\left(4\pi B(T) - \varphi\right), & (\boldsymbol{x}, t) \in \Omega \times [0, t_f], \\ \boldsymbol{s} \cdot \nabla\psi + (\kappa + \sigma)\,\psi &= \dfrac{\sigma}{4\pi}\varphi + \kappa B(T), & (\boldsymbol{x}, \boldsymbol{s}) \in \Omega \times \mathbb{S}^2, \\ \mathcal{K}_c \boldsymbol{n}(\hat{\boldsymbol{x}}) \cdot \nabla T + h_c(T - T_b) &= \alpha\pi\Big(B(T_b) - B(T)\Big), & (\hat{\boldsymbol{x}}, t) \in \partial\Omega \times [0, t_f], \\ \psi(\hat{\boldsymbol{x}}, \boldsymbol{s}) &= B(T_b), & (\hat{\boldsymbol{x}}, \boldsymbol{s}) \in \partial\Omega^- \times \mathbb{S}^2, \\ T(\boldsymbol{x}, 0) &= T_0(\boldsymbol{x}), & \boldsymbol{x} \in \Omega. \end{cases} \tag{13}$$

In our simulations presented in section 5, we also compare numerical results for the solutions without considering the radiation effect to those obtained with the radiation effect in grey media, and with the radiation in non-grey media. In this case, the governing equation for phase change problem without radiation are simply

$$\begin{cases} \alpha(T)\dfrac{\partial T}{\partial t} + \rho L \dfrac{\partial F_\epsilon(T)}{\partial t} - \nabla \cdot \Big(\mathcal{K}_c(T)\nabla T\Big) &= 0, & (\boldsymbol{x}, t) \in \Omega \times [0, t_f], \\ \mathcal{K}_c \boldsymbol{n}(\hat{\boldsymbol{x}}) \cdot \nabla T + h_c(T - T_b) &= 0, & (\boldsymbol{x}, t) \in \partial\Omega \times [0, t_f], \\ T(\boldsymbol{x}, 0) &= T_0(\boldsymbol{x}), & \boldsymbol{x} \in \Omega. \end{cases} \tag{14}$$

Note that the system (14) has been subject to several studies in the literature, see [20, 21, 33] among others. Numerical results obtained for the system (14) have been verified against analytical solutions in [20] for two-dimensional problems and in [21] for three-dimensional problems. Validation of the system (14) using experimental data has also been reported in [33]. The system (14) has also been coupled with Rosseland approximation in [34].

3. Numerical methods and solution procedure

In this section we formulate numerical methods used for solving the coupled radiative and conductive heat transfer in a non-grey absorbing and emitting media under phase change governed by the system (7)-(8). Here, the discrete ordinates method is implemented for the angle discretization, a weighted discretization on staggered grids is used for the space discretization, and a fully implicit integration scheme is applied for the time discretization. In fact, assuming S_{N_s} as the set of discrete directions is selected for the angle discretization in the unit sphere $\mathbb{S}^2$ the two-dimensional ordinates set is achieved by the simplification of one direction in S_{N_s} such that the simplified set is symmetric, has

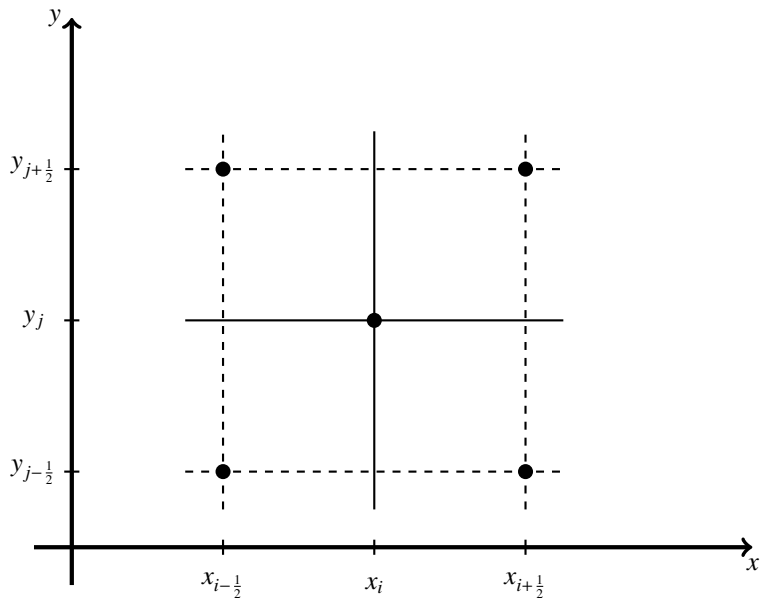

Figure 1: The staggered grid used for the space discretization in the present study.

nonzero direction, and with positive weights. Thus, a semi-discrete formulation of the two-dimensional radiative transfer equation in (7)-(8) is given by

$$\begin{aligned} \mu_l \frac{\partial \psi_l}{\partial x} + \eta_l \frac{\partial \psi_l}{\partial y} + (\sigma + \kappa)\psi_l &= \sigma\varphi(x,y) + q_l(x,y), \quad \text{in} \quad \Omega \times S_{N_s}, \\ \psi_l(x,y) &= G_l(x,y), \qquad\qquad\quad \text{on} \quad \partial\Omega^- \times S_{N_s}, \end{aligned} \tag{15}$$

where $\psi_l(x,y)$, $Q_l(x,y)$ and $G_l(x,y)$ are approximations to $\psi(x,y,\mu_l,\eta_l)$, $q(x,y,\mu_l,\eta_l)$ and $G(x,y,\mu_l,\eta_l)$, respectively. Here, the source terms q and G are defined according to the problem (7)-(8) as $q = \kappa B(T)$ and $G = B(T_b)$. Note that the angular discretization (15) transforms the original integro-differential equation in (7)-(8) into a system of N_s coupled differential equations. The method is widely used in computational radiative transfer and well documented in the literature, we refer the reader to [35] for detailed implementation of the method.

In the current study, using the transport nature of the equations (15), we consider a space discretization based on volume controls and cell averaging using upwinding techniques. For simplicity in the presentation, we assume rectangular space domain $\Omega = [x_L, x_R] \times [y_B, y_T]$ with the numerical mesh defined as

$$\Omega_h = \left\{ \boldsymbol{x}_{ij} = (x_i, y_j)^\top, \quad x_i = x_L + i\Delta x, y_j = y_B + j\Delta y, \quad i = 0, 1, \ldots, N, \quad j = 0, 1, \ldots, M \right\},$$

with h denotes the maximum cell size $h = \max(\Delta x, \Delta y)$. We also define the averaged gridpoints as

$$\Delta x = x_{i+1} - x_i, \quad \Delta y = y_{j+1} - y_j, \quad x_{i+\frac{1}{2}} = \frac{x_{i+1} + x_i}{2}, \quad y_{j+\frac{1}{2}} = \frac{y_{j+1} + y_j}{2}.$$

We use the notation W_{ij} to denote the approximation value of a generic function W at the gridpoint (x_i, y_j). Using the

semi-discrete formulation (15), a fully discrete approximation for the equation (7)-(8) can be formulated as

$$\mu_l \frac{\psi_{l,i+1j} - \psi_{l,ij}}{\Delta x} + \eta_l \frac{\psi_{l,ij+1} - \psi_{l,ij}}{\Delta y} + (\sigma_{i+\frac{1}{2}j+\frac{1}{2}} + \kappa_{i+\frac{1}{2}j+\frac{1}{2}})\psi_{l,i+\frac{1}{2}j+\frac{1}{2}} = \sigma_{i+\frac{1}{2}j+\frac{1}{2}}\varphi_{i+\frac{1}{2}j+\frac{1}{2}} + q_{l,i+\frac{1}{2}j+\frac{1}{2}}, \tag{16}$$

where the cell averaged approximations of the radiative intensity ψ are defined by

$$\begin{aligned} \psi_{l,i+1j} &= \frac{1}{\Delta x}\int_{y_j}^{y_{j+1}} \psi_l(x_i, y)dy, \\ \psi_{l,ij+1} &= \frac{1}{\Delta y}\int_{x_i}^{x_{i+1}} \psi_l(x, y_j)dx, \\ \psi_{l,ij} &= \frac{1}{\Delta x \Delta y}\int_{x_i}^{x_{i+1}}\int_{y_j}^{y_{j+1}} \psi_l(x, y)dxdy. \end{aligned} \tag{17}$$

Next, to approximate the fluxes (17), we use the well-established Diamond difference method which consists on centred differences and approximating the function values at the cell centres by averaging their values at the neighbouring nodes, see Figure 1 for an illustration of the grids used in the present study. Thus, values of the function $W_{i+\frac{1}{2}j+\frac{1}{2}}$ at the cell centre are simply approximated by a bilinear interpolation as

$$W_{i+\frac{1}{2}j+\frac{1}{2}} = \frac{W_{ij} + W_{i+ij} + W_{ij+1} + W_{i+1j+1}}{4}. \tag{18}$$

Hence, the mean radiative intensity $\varphi_{i+\frac{1}{2}j+\frac{1}{2}}$ in (16) is defined as

$$\varphi_{i+\frac{1}{2}j+\frac{1}{2}} = \sum_{l=1}^{N_s} \omega_l \frac{\psi_{ij} + \psi_{i+ij} + \psi_{ij+1} + \psi_{i+1j+1}}{4}.$$

It should be stressed that full details on the Diamond difference method can be found in [35] and therefore are omitted here. For the space discretization of the diffusion operator in (7)-(8), a consistent second-order approximation is adopted using the same cell averaging as in the space discretization of the radiative transfer equation. Thus,

$$\nabla \cdot (\mathcal{K}\nabla T)\Big|_{ij} \approx \mathcal{D}_h^2 (\mathcal{K}_c T)_{ij}, \tag{19}$$

where the difference operator $\mathcal{D}_h^2$ is given by $\mathcal{D}_h^2 = \mathcal{D}_x^2 + \mathcal{D}_y^2$, with

$$\begin{aligned} \mathcal{D}_x^2 (\mathcal{K}_c T)_{ij} &= \frac{\mathcal{K}_{c_{ij}} + \mathcal{K}_{c_{i+1j}}}{2}\frac{T_{i+1j} - T_{ij}}{(\Delta x)^2} - \frac{\mathcal{K}_{c_{i-1j}} + \mathcal{K}_{c_{ij}}}{2}\frac{T_{ij} - T_{i-1j}}{(\Delta x)^2}, \\ \mathcal{D}_y^2 (\mathcal{K}_c T)_{ij} &= \frac{\mathcal{K}_{c_{ij}} + \mathcal{K}_{c_{ij+1}}}{2}\frac{T_{ij+1} - T_{ij}}{(\Delta y)^2} - \frac{\mathcal{K}_{c_{ij-1}} + \mathcal{K}_{c_{ij}}}{2}\frac{T_{ij} - T_{ij-1}}{(\Delta y)^2}. \end{aligned}$$

Hence, the space discretization of the heat conduction equation (7)-(8) yields

$$\alpha\left(T_{i+\frac{1}{2}j+\frac{1}{2}}\right)\frac{dT_{i+\frac{1}{2}j+\frac{1}{2}}}{dt} + \rho L\frac{dF_\epsilon\left(T_{i+\frac{1}{2}j+\frac{1}{2}}\right)}{dt} - \mathcal{D}_h^2 (\mathcal{K}_c T)_{ij} = -\sum_{k=1}^{N_f} \kappa_k \left(4\pi B^{(k)}\left(T_{i+\frac{1}{2}j+\frac{1}{2}}\right) - \varphi^{(k)}_{i+\frac{1}{2}j+\frac{1}{2}}\right), \tag{20}$$

and the approximations $T_{i+\frac{1}{2}j+\frac{1}{2}}$ and $\varphi^{(k)}_{i+\frac{1}{2}j+\frac{1}{2}}$ are defined in (18). Finaly, to integrate the semi-discrete system (20) in

Table 1: Reference parameters used in our simulations for accuracy test example.

Material quantity	Reference value	Material quantity	Reference value
$\mathcal{K}_s$	$0.1\ W \cdot m^{-1} \cdot K^{-1}$	c_s	$1\ J \cdot kg^{-1} \cdot K$
$\mathcal{K}_l$	$0.1\ W \cdot m^{-1} \cdot K^{-1}$	c_l	$1\ J \cdot kg^{-1} \cdot K$
ρ	$1\ kg \cdot m^{-3}$	ϵ	1
L	$1\ J \cdot kg^{-1}$	a_R	$5.67 \times 10^{-8}\ W \cdot m^{-2} \cdot K^4$
κ	$1\ m^{-1}$	σ	$1\ m^{-1}$
T_f	$0\ K$		

time we consider a second-order implicit backward differentiation formula (BDF2) also known by Gear scheme as

$$\alpha\left(T^{n+1}_{i+\frac{1}{2}j+\frac{1}{2}}\right)\frac{3T^{n+1}_{i+\frac{1}{2}j+\frac{1}{2}} - 4T^{n}_{i+\frac{1}{2}j+\frac{1}{2}} + T^{n-1}_{i+\frac{1}{2}j+\frac{1}{2}}}{2\Delta t} - \mathcal{D}_h^2\left(\mathcal{K}T^{n+1}\right)_{ij} =$$

$$-\rho L\frac{3F_\epsilon\left(T^{n+1}_{i+\frac{1}{2}j+\frac{1}{2}}\right) - 4F_\epsilon\left(T^{n}_{i+\frac{1}{2}j+\frac{1}{2}}\right) + F_\epsilon\left(T^{n-1}_{i+\frac{1}{2}j+\frac{1}{2}}\right)}{2\Delta t} - \sum_{k=1}^{N_f}\kappa_k\left(4\pi B^{(k)}\left(T^{n+1}_{i+\frac{1}{2}j+\frac{1}{2}}\right) - \varphi^{(k)}_{i+\frac{1}{2}j+\frac{1}{2}}\right). \tag{21}$$

It is clear that the fully discrete system (21) results in a nonlinear system of algebraic equations to be solved for T^{n+1} at each timestep. In our simulations, a Newton-Raphson algorithm equipped with a residual norm less than 10^{-6} for the convergence is implemented.

4. Numerical results and examples

To demonstrate the performance of the methodology presented in this study, we numerically solve the proposed phase-change-radiative-transfer model to study effects of radiation in phase change materials. Three test problems are considered in this section and numerical results are discussed for different radiative regimes. We first check the convergence of our algorithm using a problem with a known manufactured analytical solution. Next, we consider two solidification examples to illustrate effects of radiation in the temperature distribution during the process of steel continuous casting. In all our simulations, the S_8 set is used for the discretization of the unit sphere $\mathbb{S}^2$ which yields $N_s = 80$ but other S_n discrete-ordinates sets from [36] can also be used.

4.1. Accuracy test example

In this example, we aim to quantify the convergence rates in space and time for the proposed numerical techniques. To this end, we solve the coupled problem (13) in the squared domain $\Omega = [0, 1] \times [0, 1]$ and final time $t = 1$ using

Table 2: Convergence results for the accuracy example using different timesteps Δt at time $t = 1$.

Δt	$\| e \|_{L^\infty}$	Rate	$\| e \|_{L^1}$	Rate	$\| e \|_{L^2}$	Rate
0.2	1.8000E-03	—	1.9000E-03	—	2.3000E-03	—
0.1	4.4870E-04	2.0042	4.9335E-04	1.9453	6.0250E-04	1.9326
0.05	1.1006E-04	2.0275	1.2141E-04	2.0227	1.4905E-04	2.0152
0.025	2.5398E-05	2.1155	2.7960E-05	2.1185	3.4237E-05	2.1222

Table 3: Convergence results for the accuracy example using different space steps $h = \Delta x = \Delta y$ at time $t = 1$.

h	$\| e \|_{L^\infty}$	Rate	$\| e \|_{L^1}$	Rate	$\| e \|_{L^2}$	Rate
0.2	8.3900E-02	—	1.2480E-01	—	1.6460E-01	—
0.1	2.3800E-02	1.8177	3.0500E-02	2.0327	4.3500E-02	1.9199
0.05	6.6000E-03	1.8504	7.8000E-03	1.9673	1.0600E-02	2.0370
0.025	1.7000E-03	1.9569	2.0000E-03	1.9635	2.6000E-03	2.0275

the parameters listed in Table 1. The right-hand functions along with the boundary functions T_b and ψ_b, and the initial function T_0 are explicitly calculated such that the exact solution of the equations (13) is given by

$$T_a(x, y, t) = \sin(2\pi x)\cos(2\pi y)\exp(-t), \qquad \psi_a(x, y, \mu, \eta) = x^2y^2(1 - x^2)(1 - y^2)(1 + \mu^2 + \eta^2).$$

We also define the relative L^∞-, L^1- and L^2-errors as

$$\| e \|_{L^\infty} = \frac{\|T - T_a\|_{L^\infty}}{\|T_a\|_{L^\infty}}, \quad \| e \|_{L^1} = \frac{\|T - T_a\|_{L^1}}{\|T_a\|_{L^1}}, \quad \| e \|_{L^2} = \frac{\|T - T_a\|_{L^2}}{\|T_a\|_{L^2}},$$

where T_a and T are the analytical and numerical solutions, respectively. To verify the convergence in time, we use a fine uniform mesh with $h = \Delta x = \Delta y = 0.001$ and then, we consider four timesteps Δt of different sizes. Table 2 presents the obtained errors along with the associated convergence rates. It is clear that for the considered example, decreasing the timestep results in a decrease of all errors and a second-order convergence is achieved in the proposed time integration method solving this accuracy test example.

Similarly, to examine the space convergence in the proposed method, we use a small timestep $\Delta t = 0.0025$ and then, we consider four uniform meshes with different values of the spatial discretization step h. The obtained results for the considered errors along with the convergence rates are presented in Table 3. Again, refining the mesh results in a decrease in all errors and the method exhibits a second-order convergence in all considered norms. It is evident that a second-order accuracy in both time and space has been obtained for this test problem with known analytical

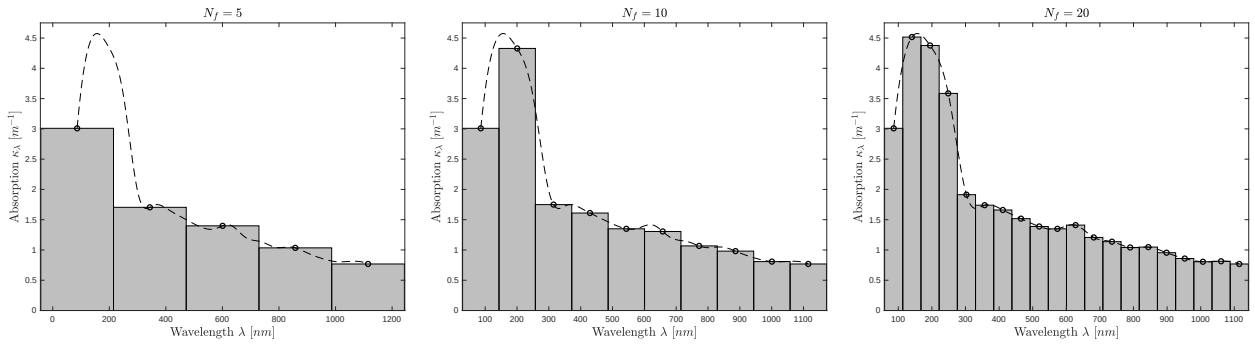

Figure 2: Spectral absorption coefficients used in this study for the solidification problem of a continuous cast steel Alloy with the spectrum divided into 5 bands (left plot), 10 bands (middle plot) and 20 bands (right plot).

Table 4: Reference parameters used in our simulations for Case 1 in the solidification problem of a continuous cast steel Alloy.

Material quantity	Reference value	Material quantity	Reference value
$\mathcal{K}_s$	$36.6\ W \cdot m^{-1} \cdot K^{-1}$	c_s	$682.0\ J \cdot kg^{-1} \cdot K$
$\mathcal{K}_l$	$256.2\ W \cdot m^{-1} \cdot K^{-1}$	c_l	$710.0\ J \cdot kg^{-1} \cdot K$
ρ	$7400\ kg \cdot m^{-3}$	ϵ	22.5
L	$272000\ J \cdot kg^{-1}$	a_R	$5.67 \times 10^{-8}\ W \cdot m^{-2} \cdot K^4$
T_0	$1845\ K$	T_f	$1772.5\ K$
T_b	$500\ K$	h_c	$1000\ J \cdot kg^{-1} \cdot K^{-1}$

solutions.

4.2. Solidification problem of a continuous cast steel Alloy

In this example we consider the solidification problem of a continuous cast steel Alloy in two different enclosures using different material properties. These problems are well-established and widely used in the literature for solidification problems of continuous cast steel, see for instance [37, 15]. It should be stressed that the primary zone in the continuous casting process undergoes the highest temperature difference. In addition, at this zone a liquid metal is continuously supplied to the mould and the liquid metal solidifies on the boundary yielding the initial shape of the steel beam. Therefore, the radiation in this zone is expected to substantially influence both the solid-liquid interface and the thermal features in the mould due to the high temperature involved in this process. Thus, accurate numerical modelling of this process is essential for enhancing the productivity of the steel casting. In Figure 2 we present the spectrum used in our computations for the solidification of a continuous cast steel Alloy [38]. Here, the spectrum is divided into $N_f = 5$, 10 and 20 bands with piecewise constant absorption coefficients as shown in this figure.

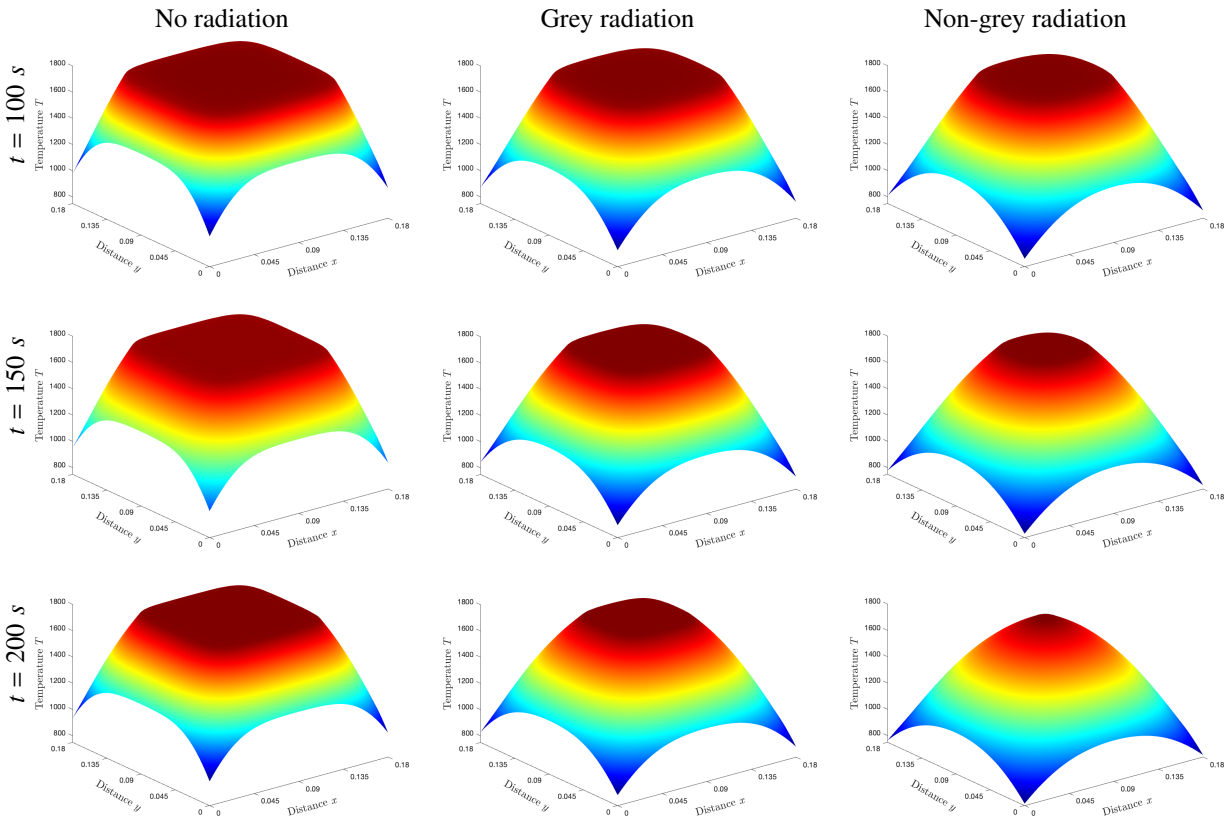

Figure 3: Temperature obtained for Case 1 in the solidification problem of a continuous cast steel Alloy using no radiation (first column), grey radiation (second column) and non-grey radiation (third column) at time $t = 100\ s$ (first row), $t = 150\ s$ (second row) and $t = 200\ s$ (third row).

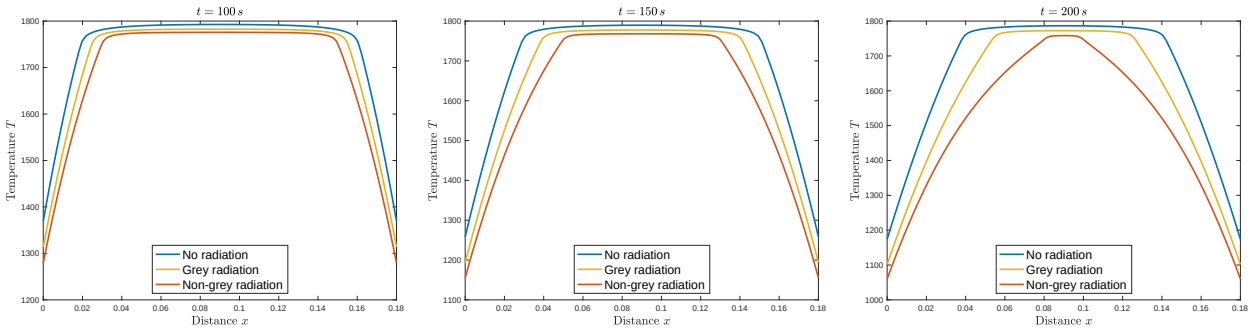

Figure 4: Cross-sections of the temperature at the horizontal centerline in the computational domain for Case 1 in the solidification problem of a continuous cast steel Alloy at the three selected instants $t = 100\ s$ (left), $t = 150\ s$ (middle) and $t = 200\ s$ (right).

Depending on the geometry and the thermal characteristics of the material, the following cases are selected.

4.2.1. Case study 1

We first consider the test example of solidification process of a steel billet in a continuous casting strand (in the primary zone). This problem has been used as a benchmark for the solidification problems in [37] but without

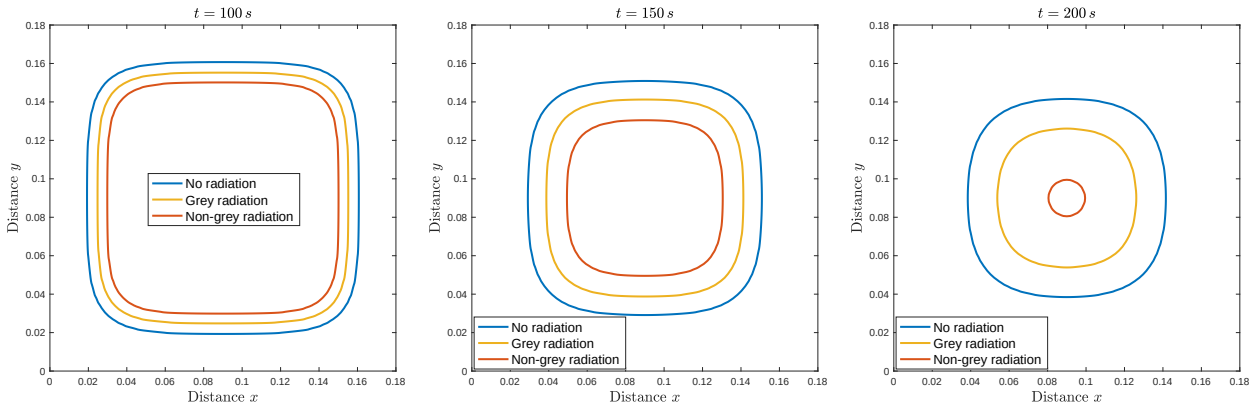

Figure 5: Interface position for Case 1 in the solidification problem of a continuous cast steel Alloy at the three selected instants $t = 100\ s$ (left), $t = 150\ s$ (middle) and $t = 200\ s$ (right).

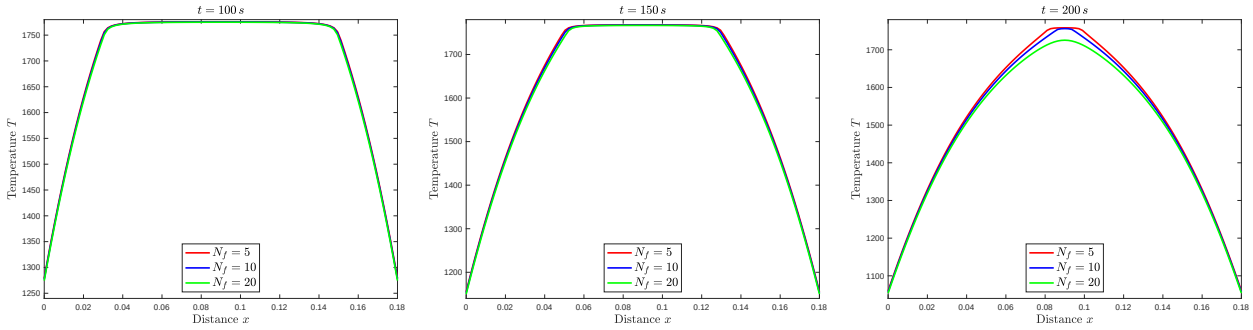

Figure 6: Cross-sections of the temperature at the horizontal centerline in the computational domain for Case 1 in the solidification problem of a continuous cast steel Alloy obtained with non-grey radiation using different numbers of bands in the optical spectrum at the three selected instants $t = 100\ s$ (left), $t = 150\ s$ (middle) and $t = 200\ s$ (right).

accounting of radiation effects. The computational domain consists of a squared plate 0.18 m long and 0.18 m wide. The temperature of the molten steel is assumed to be 1845 K at the start, which is higher than the liquidus temperature of 1795 K while the temperature of the solidus is 1750 K. We consider the Robin-type boundary conditions with a heat transfer coefficient of $h_c = 1000\ W\ m^2/K$ and the ambient temperature is set to $T_b = 500\ K$. In this example, the steel is assumed to be non-grey absorbing and non-scattering media with the spectral absorption coefficients given in Figure 2. In all computations reported for this case, the selected values for the evaluation of the present models are taken from [37] and summarized in Table 4. Note that for the grey simulations, a single absorption coefficient fixed to $\kappa = 1$ is used in the simulations along with the parameters listed in Table 4.

Figure 3 depicts the temperature distributions obtained using for simulations with no radiation, grey radiation and non-grey radiation with 20 bands. Here, a uniform mesh with 100×100 gridpoints is used in all simulations along with a timestep $\Delta t = 0.1\ s$ and the computed results are presented at three different instants namely, $t = 100\ s$, 150 s and 200 s. For comparison reasons, we display in Figure 4 cross-sections of these temperature distributions at the horizontal centerline of the computational domain corresponding to $y = 0.09\ m$. It is evident that the proposed

Table 5: Reference parameters used in our simulations for Case 2 in the solidification problem of a continuous cast steel Alloy.

Material quantity	Reference value	Material quantity	Reference value
$\mathcal{K}_s$	$2.268\ W \cdot m^{-1} \cdot K^{-1}$	c_s	$1\ J \cdot kg^{-1} \cdot K$
$\mathcal{K}_l$	$1.3608\ W \cdot m^{-1} \cdot K^{-1}$	c_l	$1.2\ J \cdot kg^{-1} \cdot K$
ρ	$1000\ kg \cdot m^{-3}$	ϵ	100
L	$1000\ J \cdot kg^{-1}$	a_R	$5.67 \times 10^{-8}\ W \cdot m^{-2} \cdot K^4$
T_f	$700\ K$	σ	$9\ m^{-1}$
T_0	$1000\ K$		

numerical techniques perform well as the solidification process is clearly captured for this case of simulations with and without radiation. It should be pointed out that results in Figure 4 obtained for simulations without radiation agree well with those reported in [37]. It is also evident from the results shown in Figure 3 and Figure 4 that the radiation effects in both simulations with grey and non-grey radiations alter the temperature distributions as clearly shown in the temperature profiles. As the time progresses, these differences in the temperature profiles become more pronounced, see for example the results at $t = 200\ s$ in Figure 4.

Under the considered radiative conditions, the inclusion of radiation in these models results in an accelerated solidification process and the material is shown to be colder at the domain boundaries. Furthermore, the radiation in this case has decreased the temperature in the liquid phase and impacted the location of the liquid-solid interface. To illustrate these effects, we present in Figure 5 the obtained results for the liquid-solid interface for simulations with and without radiation at the three selected times. It is clear that the interface liquid-solid has been influenced by the radiative effects obtained using both grey and non-grey simulations. These results confirm the importance of the thermal radiation in this solidification problem of a continuous cast steel Alloy for which these radiative effects should be accounted for in its modelling and simulation.

As a final concern for this case, we examine the effects of finite spectral bands in the computed temperature using non-grey simulations. For this end we consider the spectral divisions with the number of bands $N_f = 5$, $N_f = 10$ and $N_f = 20$ as shown in Figure 2. In Figure 6, we present cross-sections of the temperature distributions at the horizontal centerline $y = 0.09\ m$ using the considered frequency bands. It is observed that the temperature profile has slightly changed depending on the number of frequency bands in the spectrum. Notice that our proposed model has the flexibility to consider several frequency bands in the optical spectrum depending on the spectral absorption of the material. In the situation of steel Alloy, we have found that 20 bands in the optical spectrum are enough to obtain results free from the frequency effects at a reasonable accuracy. In this example, we have clearly demonstrated the impact of the material spectrum on both the liquid-solid interface and the temperature profile. This highlights the

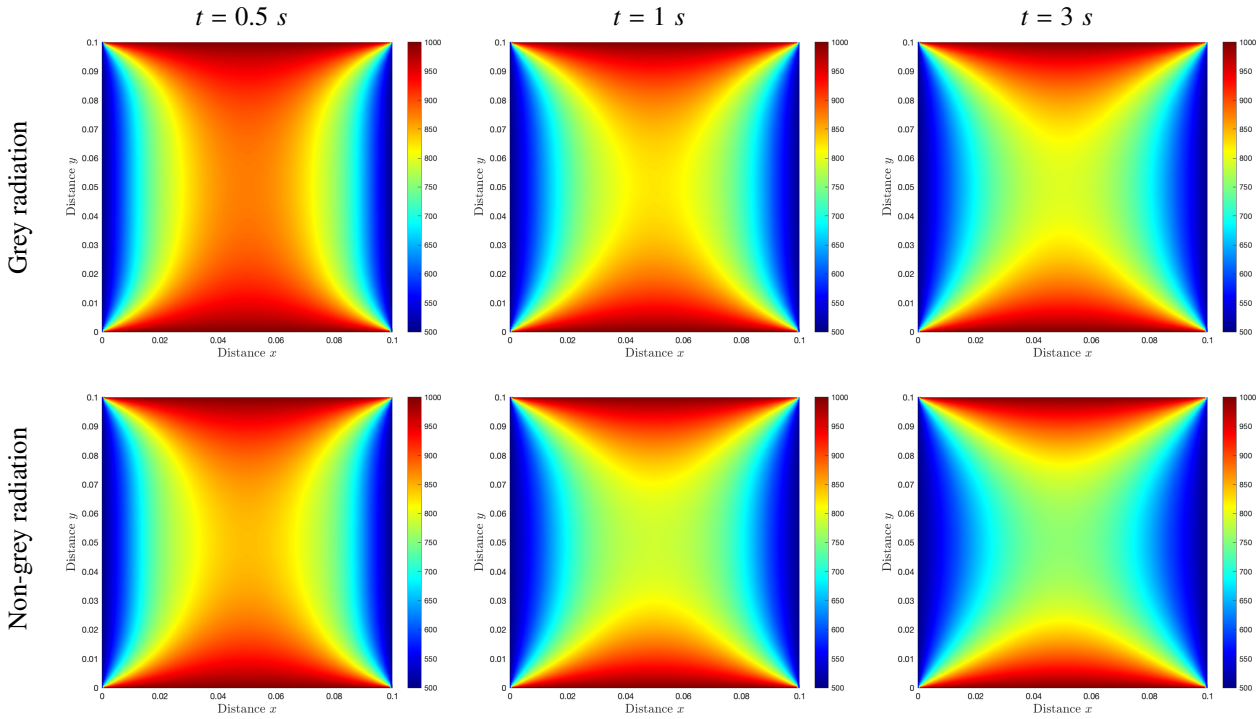

Figure 7: Temperature obtained for Case 2 in the solidification problem of a continuous cast steel Alloy using grey radiation (first row) and non-grey radiation (second row) at time $t = 0.5\ s$ (first column), $t = 1\ s$ (second column) and $t = 3\ s$ (third column).

significance of our proposed model, which effectively incorporates frequencies into the phase-change equations. The importance of this model becomes even more pronounced in materials with substantial frequency variations in the optical spectral as observed in glass manufacturing among others.

4.2.2. Case study 2

In this case, we consider another situation of the solidification process of the steel in a continuous casting strand as before but in a scattering medium with different thermal properties. Here, we solve the proposed models in a squared domain 0.1 m long on both sides and using the parameters presented in Table 5. This benchmark problem has been used in [15] to investigate impact of the refractive index on the solidification heat transfer in the semi-transparent medium. In our case, we assume the refractive index constant to be equal to one and the parameters of thermophysical properties are considered to be different in each phase, whereas those of radiative properties are supposed to be the same. The squared enclosure is initially filled with the liquid at temperature $T_0 = 1000\ K$ which is higher than the freezing temperature $T_f = 700\ K$. The top and bottom boundaries of the enclosure are kept at fixed temperature $T_b = 1000\ K$ while the left and right walls of the enclosure are kept at temperature $T_b = 500\ K$. Table 5 summarizes values of the involved parameters selected in this case for the evaluation of the present models. Here, only the 10 frequency bands shown in Figure 2 are used in the non-grey simulations whereas, for the grey simulations, a single

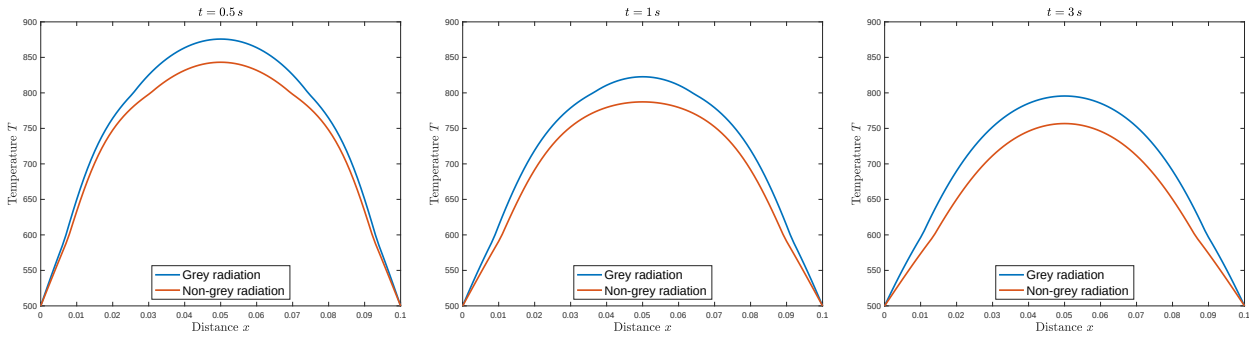

Figure 8: Cross-sections of the temperature at the horizontal centerline in the computational domain for Case 2 in the solidification problem of a continuous cast steel Alloy at the three selected instants $t = 0.5\ s$ (left), $t = 1\ s$ (middle) and $t = 3\ s$ (right).

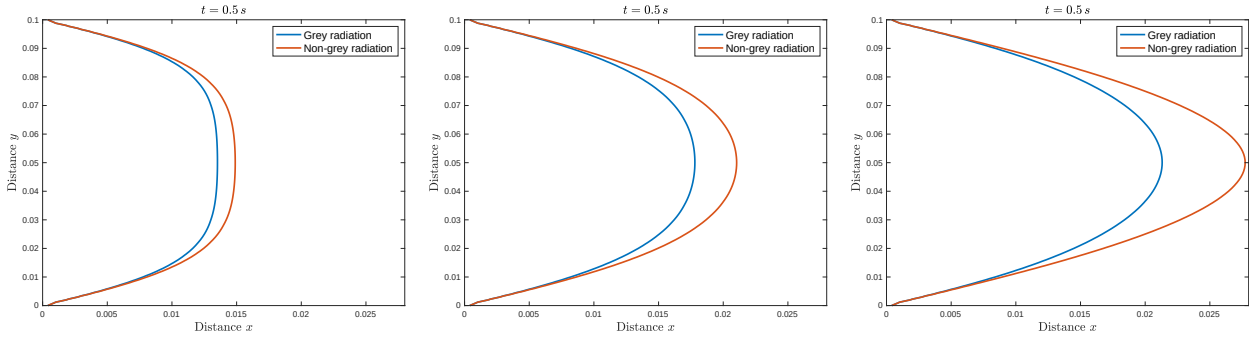

Figure 9: Interface positions at the left side of the computational domain for Case 2 in the solidification problem of a continuous cast steel Alloy at the three selected instants $t = 0.5\ s$ (left), $t = 1\ s$ (middle) and $t = 3\ s$ (right).

absorption coefficient fixed to $\kappa = 1$ is used in this case. It should be noted that compared to the previous case, the present case involves scattering in addition to the absorbing and emitting media at fixed boundary conditions. Therefore, a faster solidification process is expected for this case than Case 1. Here, the spatial domain is discretized using a uniform mesh with 100×100 gridpoints, the timestep Δt is fixed to $0.01\ \ s$, and the computed results are presented at times $t = 0.5\ s$, $1\ s$ and $3\ s$.

In Figure 7 we display the temperature distributions obtained for simulations with grey radiation and non-grey radiation. Figure 8 illustrates cross-sections of these temperature distributions at the horizontal centerline in the computational domain with $y = 0.05\ m$. As in the previous simulations for Case 1, accounting for radiation in both grey and non-grey regimes, the temperature distribution exhibits different patterns with consistent changes in its profile along the horizontal centerline. It should also be stressed that our results obtained for this case with grey radiation are in agreement with those obtained for the same solidification benchmark problem in [15]. Apparently, the overall thermal features of the considered material for this solidification problem are accurately resolved using the proposed computational method with no spurious oscillations appearing in the numerical results.

For further investigations of the radiative effects on the temperature and its evolution within time, liquid-solid

Table 6: Percentage of the computational cost used by each stage of grey radiation and non-grey radiation, using the time for the first 10 steps. The CPU times are given in seconds.

		Grey radiation		Non-grey radiation	
Stage	Algorithm	CPU	Percentage	CPU	Percentage
Radiation Stage	Assemblage	0.11	2.60%	0.57	6.74%
	Source Iteration	0.85	20.09%	3.39	40.07%
	Total	0.96	22.69%	3.96	46.81%
Phage-change Stage	Jacobian	2.71	64.07%	3.38	39.95%
	RHS	0.08	1.89%	0.06	7.68%
	Solving System	0.48	11.35%	0.47	5.56%
	Total	3.27	77.31%	4.50	53.19%
Total		4.23	100%	8.46	100%

interfaces are illustrated in Figure 9 for the considered simulations at the selected times. For a better insight, only the interfaces in the left side of the computational domain are displayed in this figure as those interfaces in the right side present similar structures. It is clear from these results that the change in the temperature profile due to the presence of radiation has also affected the liquid-solid interface which is an important feature in phase-change problems. As in Case 1, it has been demonstrated in this case that a substantial frequency variation in the material would affect both the liquid-solid interface and the temperature profile. This endorses the significance of our proposed model in incorporating frequencies into the phase-change equations. The proposed mathematical models and numerical methods perform well for this solidification problem of a continuous cast steel Alloy as they accurately capture the thermal features of the material without the requirement of complicated computational techniques for representations of the radiative heat transfer in non-grey absorbing and emitting media under phase change.

Analysis of computational cost has also been carried out in this case study. In Table 6 we summarize the computational cost of the grey and non-grey simulations using the same parameters as before. Here, the computational cost is divided into two stages. The first stage is the radiation stage, which involves solving the radiation problem. This includes Assemblage, representing the percentage of CPU time used for assembling vectors and matrices in the solution of radiative transfer equation. Source Iterations, indicating the CPU time allocated for approximating the radiative intensity. The second stage focuses on solving the phase-change heat conduction, referred to as the Phase-change stage. This includes Jacobian, representing the percentage of CPU time spent calculating the Jacobian in the Newton system. RHS, refers to the CPU time used for calculating the right-hand side term in the Newton system. Solving System, representing the percentage of CPU time dedicated to solving the Newton system. Total refers to the percentage of CPU time required for solving each stage. The last column presents the total CPU time for both stages combined. The main features reported in this table are on one hand, the full radiative step requires less computational cost compared

to the CPU time needed for the Newton solver for the grey media case. On the other hand, the full radiative step is an important step when it comes to simulations of the non-grey media. This is expected as the model adds more accuracy to the solution by adding more integral terms. As can be seen from Table 6, a considerable computational effort goes into the Newton algorithm solving the associated nonlinear problems. Therefore, reducing the CPU time in the proposed method can be achieved by constructing more efficient preconditioned iterative solvers for the nonlinear systems. For instance, multilevel techniques are known to be the most efficient methods for solving linear and nonlinear systems and can therefore be the suitable tools to increase the efficiency of the proposed method. Needless to say that the CPU time in Table 6 can drastically be reduced if parallel computers are used. A parallel method can be implemented using the message passing interface (MPI). This parallel efficiency using the MPI becomes very high when the discrete ordinates lie within the local memory of the same processor and the operation per processor is kept constant.

5. Conclusions

In this paper, we have presented a class of mathematical models for modelling and numerical simulation of the coupling phase-change heat transfer and radiation in a non-grey absorbing and emitting media. The proposed model employs the enthalpy technique for phase change in materials coupled to a set of nonlinear integro-differential equations accounting for thermal radiation. For non-grey media, the optical spectrum is divided into a finite set of bands with averaged absorption and scattering coefficients. A second-order method is implemented for the space and time discretizations of the coupled equations. For the angular discretization of the integral equation for the radiation effects, we used discrete ordinates and a Newton-type algorithm was adopted to deal with the nonlinear systems. Numerical results are presented for two test problems in both grey and non-grey media, and comparisons to simulation without radiation have also been performed. For the considered problems and under the selected radiative transfer conditions, it has been found that the radiation effects decreased the temperature in the liquid and accelerated the solidification process of the medium. Needless to mention that changes in the temperature profile have also affected positions of the liquid-solid interface in these problems. Although we have restricted our numerical simulations to the two-dimensional phase change problems, the proposed techniques can be extended to model radiative heat transfer in non-grey absorbing and emitting media under phase change in three space dimensions. Furthermore, in many practical problems in radiative heat transfer, the involved parameters are not constant and the medium is not isotropic homogeneous. The presence of high temperatures in these applications can be conveniently described by nonlinear relations, whose parameters are mainly inferred from experiments. This requires to include, in the governing partial differential equations modeling the problem under study, a rational assessment of nonlinear anisotropy. Developing robust numerical tools for solving these problems is of great interest. Coupling convection and radiation in non-grey, absorbing, and emitting media under phase change presents a significant challenge [39, 40]. Nonetheless, these and related issues will be explored in future investigations.

Acknowledgment

The authors wish to acknowledge the financial support provided by the Royal Society under the contract IES-R2-202078 and the financial support provided by the American University of Sharjah.

Data availability statement

The data that support the findings of this study are available from the corresponding author upon reasonable request.

Conflict of interest

The authors have no competing interests to declare that are relevant to the content of this paper.

References

[1] P. Barral, L. Pérez-Pérez, P. Quintela, Transient thermal response with nonlocal radiation of a blast furnace main trough, Applied Mathematical Modelling 105 (2022) 197–225.

[2] D. Szeliga, K. Kubiak, G. Jarczyk, The influence of the radiation baffle on predicted temperature gradient in single crystal cmsx-4 castings, International Journal of Metalcasting 7 (2013) 17–23.

[3] A. G. Fedorov, L. Pilon, Glass foams: formation, transport properties, and heat, mass, and radiation transfer, Journal of Non-Crystalline Solids 311 (2) (2002) 154–173.

[4] V. Kez, F. Liu, J. Consalvi, J. Ströhle, B. Epple, A comprehensive evaluation of different radiation models in a gas turbine combustor under conditions of oxy-fuel combustion with dry recycle, Journal of Quantitative Spectroscopy and Radiative Transfer 172 (2016) 121–133.

[5] M. Izadi, Y. Belhamadia, S. Dubljevic, Dynamical analysis of melt flow in the bridgman process, Industrial & Engineering Chemistry Research 53 (45) (2014) 17811–17817.

[6] Y. Belhamadia, G. O. Cassol, S. Dubljevic, Numerical modelling of hyperbolic phase change problems: Application to continuous casting, International Journal of Heat and Mass Transfer 209 (2023) 124042.

[7] G. B. Lebon, H.-T. Li, J. B. Patel, H. Assadi, Z. Fan, Numerical modelling of melt-conditioned direct-chill casting, Applied Mathematical Modelling 77 (2020) 1310–1330.

[8] J. Stefan, Uber die theorie der eisbildung, insbesondere fiber die eisbildung im polarmeere, Annalen der Physik und Chemie 42 (1891) 269–286.

[9] M. Abrams, R. Viskanta, The effects of radiative heat transfer upon the melting and solidification of semitransparent crystals, ASME. J. Heat Transfer 96 (2) (May 1974) 184–190.

[10] J. D. Q. Xiao, The role of internal radiation and melt convection in czochralski oxide growth: deep interfaces, interface inversion, and spiraling, J. Crystal Growth 128 (1976) 188–194.

[11] C. D. H. Chan, S. H., G. Kocamustafaogullari, Melting and solidification with internal radiative transfer-a generalized phase change model, Int. J. Heat Mass Transfer, 26 (4) (1983) 621–633.

[12] B. Y. Kwang S. Kim, Thermal radiation heat transfer effects on solidification of finite concentric cylinder medium-enthalpy model and p-1 approximation, Numerical Heat Transfer 14 (4) (1988) 483–498.

[13] F. P. Lapka, P., Numerical modelling of solidification processes of semitransparent materials using the enthalpy and the finite volume methods, Heat Mass Transfer 44 (8) (2008) 937–957.

[14] P. Lapka, P. Furmański, Fixed grid simulation of radiation-conduction dominated solidification process, ASME. J. Heat Transfer 132 (2) (February 2010) 023504.

[15] Y. Z. Hong-Liang Yi, He-Ping Tan, Coupled radiation and solidification heat transfer inside a graded index medium by finite element method, International Journal of Heat and Mass Transfer 54 (2011) 3090–3095.

[16] F. K. M. C. J. V. Johann Miranda Fuentes, Kévyn Johannes, Melting with convection and radiation in a participating phase change material, Applied Energy 109 (2013) 454–461.

[17] S.-C. S. L.-M. R. H.-P. T. Biao Zhang, Hong Qi, Solving inverse problems of radiative heat transfer and phase change in semitransparent medium by using improved quantum particle swarm optimization, International Journal of Heat and Mass Transfer 85 (2015) 300–310.

[18] J. M. Z. T. Zhenzong HE, Jiaoying HU, Estimation of radiative heat transfer and phase change in participating medium from td radiation measurement signals with pca approach, Journal of Computational Physics 14 (2) (2019) JTST0019.

[19] R. Backofen, T. Bilz, A. Ribalta, A. Voigt, SP_N-approximations of internal radiation in crystal growth of optical materials, J. Crystal Growth. 266 (2004) 264–270.

[20] Y. Belhamadia, A. Fortin, É. Chamberland, Anisotropic mesh adaptation for the solution of the Stefan problem, Journal of Computational Physics 194 (1) (2004) 233–255.

[21] Y. Belhamadia, A. Fortin, É. Chamberland, Three-dimensional anisotropic mesh adaptation for phase change problems, Journal of Computational Physics 201 (2) (2004) 753–770.

[22] D. Mihalas, B. Mihalas, Foundations of Radiation Hydrodynamics, Oxford University Press, New York, 1983.

[23] M. Modest, Radiative Heat Transfer, Third edition, Academic Press, 2013.

[24] E. Larsen, G. Thömmes, A. Klar, M. Seaid, T. Götz, Simplified P_N approximations to the equations of radiative heat transfer and applications, Journal of Computational Physics 183 (2) (2002) 652–675.

[25] A. Klar, J. Lang, M. Seaid, Adaptive solutions of SP_N-approximations to radiative heat transfer in glass, International Journal of Thermal Sciences 44 (11) (2005) 1013–1023.

[26] A. S. Fisher, S. L. Rani, A narrow band model based on the absorption coefficient and its application to the calculation of radiative transfer in one-dimensional enclosures, Journal of Quantitative Spectroscopy and Radiative Transfer 277 (2022) 107989.

[27] H. Bordbar, T. Hyppänen, Line by line based band identification for non-gray gas modeling with a banded approach, International Journal of Heat and Mass Transfer 127 (2018) 870–884.

[28] J. Marakis, Application of narrow and wide band models for radiative transfer in planar media, International journal of heat and mass transfer 44 (1) (2001) 131–142.

[29] M. F. Modest, Narrow-band and full-spectrum k-distributions for radiative heat transfer—correlated-k vs. scaling approximation, Journal of Quantitative Spectroscopy and Radiative Transfer 76 (1) (2003) 69–83.

[30] M. F. Modest, The treatment of nongray properties in radiative heat transfer: from past to present, Journal of heat transfer 135 (6) (2013) 061801.

[31] E. Larsen, G. Thömmes, A. Klar, M. Seaid, T. Götz, Simplified P_N approximations to the equations of radiative heat transfer and applications, Journal of Computational Physics 183 (2002) 652–675.

[32] A. Klar, J. Lang, M. Seaid, Adaptive solutions of SP_N-approximations to radiative heat transfer in glass, International Journal of Thermal Sciences 44 (2005) 1013–1023.

[33] A. Fortin, Y. Belhamadia, Numerical prediction of freezing fronts in cryosurgery: Comparison with experimental results, Computer methods in biomechanics and biomedical engineering 8 (4) (2005) 241–249.

[34] F.-E. Moutahir, Y. Belhamadia, M. El-Amrani, M. Seaid, Enhancing computational steel solidification by a nonlinear transient thermal model, in: D. Groen, C. de Mulatier, M. Paszynski, V. V. Krzhizhanovskaya, J. J. Dongarra, P. M. A. Sloot (Eds.), Computational Science – ICCS 2022, Springer International Publishing, Cham, 2022, pp. 305–317.

[35] M. Seaid, A. Klar, Efficient preconditioning of linear systems arising from the discretization of radiative transfer equation, in: Lecture Notes in Computational Science and Engineering, Springer, 2003, pp. 211–236.

[36] W. Fiveland, The selection of discrete ordinate quadrature sets for anisotropic scattering, ASME HTD. Fundam. Radiat. Heat Transfer. 160 (1991) 89–96.

[37] R. Tavakoli, P. Davami, Unconditionally stable fully explicit finite difference solution of solidification problems, Metall Mater Trans B 38 (2007) 121–142.

[38] J. ThomasPaulraj, A. S. Raja, J. Sathiyabama, V. Prathipa, A study of acalypha indica extract as a novel green inhibitor for carbon steel in aqueous medium, International Journal of Green and Herbal Chemistry 3 (3) (2014) 1033–1047.

[39] Y. Belhamadia, A. Fortin, T. Briffard, A two-dimensional adaptive remeshing method for solving melting and solidification problems with convection, Numerical Heat Transfer, Part A: Applications 76 (4) (2019) 179–197.

[40] M. E.-A. Jaafar Albadr, M. Seaid, Simplified pn finite element approximations for coupled natural convection and radiation heat transfer, Numerical Heat Transfer, Part A: Applications 83 (5) (2023) 478–502.